Published in final edited form as:
J Cell Mol Med. 2009 August ; 13(8B): 1920. doi:10.1111/j.1582-4934.2008.00481.x.

Raman tweezers provide the fingerprint of cells supporting the late stages of KSHV reactivation

Ossie F. Dyson[1,Ψ], **Patrick W. Ford**[1,Ψ], **De Chen**[2], **Yong-Qing Li**[2], and **Shaw M. Akula**[1,*]

[1]Department of Microbiology & Immunology, Brody School of Medicine at East Carolina University, Greenville, NC 27834.

[2]Department of Physics, East Carolina University, Greenville, NC 27858.

Abstract

Kaposi's sarcoma-associated herpesvirus (KSHV) has both latent and lytic phases of replication. The molecular switch that triggers a reactivation is still unclear. Cells from S phase of cell cycle provide apt conditions for an active reactivation. In order to specifically delineate the Raman spectra of cells supporting KSHV reactivation, we followed a novel approach where cells were sorted based on the state of infection (latent Vs lytic) by a flow cytometer and then analyzed by the Raman tweezers. The Raman bands at 785, 813, 830, 1095, and 1128 cm^{-1} are specifically altered in cells supporting KSHV reactivation. These 5 peaks make up the Raman fingerprint of cells supporting KSHV reactivation. The physiological relevance of the changes in these peaks with respect to KSHV reactivation is discussed in the following report.

Keywords

KSHV; Latency; S phase; Raman tweezers; Reactivation

INTRODUCTION

Kaposi sarcoma-associated herpesvirus (KSHV), also known as human herpesvirus-8 (HHV-8) was first described in 1994 [1]. KSHV is etiologically associated with all forms of Kaposi sarcoma (KS), primary effusion lymphoma (PEL), and multicentric Castleman disease (MCD) [2,3]. Apart from the inflammatory cytokines/growth factors, lytic KSHV infection plays an instrumental role in the progression of KS lesions [4–6]. Successful KSHV infection is characterized by both virus entry and the ability of the virus to establish latency. The lytic infection is also critical for the spread of KSHV to different organs.

KSHV infects a variety of target cells that includes human B cells, macrophages, keratinocytes, endothelial cells, and epithelial cells [7–11]. However, all of these infections are either abortive and/or latent which is characterized by the presence of circular latent viral DNA and by the expression of KSHV latency-associated nuclear antigen (LANA) encoded by ORF73 [12]. Generally, a lytic cycle of KSHV infection can be induced in cells harboring latent KSHV by treatment with phorbol-12-myristate-13-acetate (TPA) or sodium butyrate [13].

*Corresponding author: Shaw M. Akula, Department of Microbiology & Immunology, Brody School of Medicine, East Carolina University, Greenville, North Carolina, USA 27834., Phone: (252)744-2702, Fax: (252) 744-3104, Email: akulas@ecu.edu.
ΨMeans equal contribution

The concept of latency is not new to the field of herpesvirology. Herpes simplex virus (HSV; an α-herpesvirus), human cytomegalovirus (HCMV; a β-herpesvirus), and KSHV (a γ-herpesvirus) are examples of viruses from the three different herpesvirus families that cause latent infection of cells [14]. There are several other viruses that cause latent infections of target cells. Some of the other examples are hepatitis B virus, Epstein-Barr virus (EBV), and adenovirus [15,16]. Any form of stress, treatment with immunosuppressant drugs, or immune suppression has been demonstrated to reactivate herpesviruses from latency [17–19]. However, the exact mechanism for the reactivation of herpesvirus latency is still eluding. Understanding latency better will have an immediate impact on the economy as it will help us develop good anti-viral / vaccine strategies for the benefit of the mankind. For all along, relying purely on only the conventional biochemical and molecular biology approaches have not been fruitful to delineate virus latency. Knowledge on reactivation of latent virus infections in general remains limited.

Raman tweezers involves confocal microscopy, which incorporates the use of both laser (optical) tweezers and Raman spectroscopy (LTRS) [20]. The optical tweezers part of the LTRS system uses a focused near infrared (NIR) beam at 785nm to immobilize a cell while, the Raman spectroscopy part of this system uses the same NIR beam to generate the vibrational spectra of the immobilized cell. The basic steps to obtain the vibrational spectra of living cells using Raman tweezers include the following: (1) The cells will be illuminated with the NIR beam; (2) The molecules in the cells at a particular state will scatter the incident light in a specific and unique pattern; and (3) The scattered light will be collected and analyzed using a system comprising of lenses and a charge-coupled device (CCD) camera to provide the Raman spectra (detailed in the review by Lambert et al., 2006 [21]). We hypothesized that the changes in the cellular environment during different stages of virus replication will be reflected in the Raman spectra. Furthermore, if these spectral changes are specific enough for a particular stage of replication, they can, in principle, be used as a bio-marker of the replication stage. Hence, in this study we attempted to decipher the crucial fingerprints of cells capable of supporting KSHV reactivation by a combination of biochemical assays, molecular biology, and Raman tweezers.

In order to analyze KSHV reactivation, we used PEL cells (BCBL-1 and BCP-1 cells; both of which are KSHV infected human B cells) in this study. PEL cells turned out to be a blessing in disguise as they naturally harbor KSHV in a latent form and that a lytic infection may be induced conditionally by treating them with TPA [22]. Herein, we provide for the first time the Raman fingerprint of cells supporting KSHV reactivation. There are several advantages of using Raman tweezers to analyze biological specimens [21] of which the most important one with respect to the present study is the fact that it allows for the analysis of the sample without physically touching it, thereby leaving the cell in a less disturbed and more natural state [23]. Taken together, such an approach may well be exploited to understand a variety of viral infections with special emphasis to replication stages so that it may serve as a diagnostic tool in the near future.

MATERIALS AND METHODS

Cells

BCBL-1, and BCP-1 cells were used in this study. These cells were grown in phenol red-free RPMI medium (Invitrogen, Carlsbad, CA, USA) containing 10% charcoal stripped fetal bovine serum (FBS) (Atlanta Biologicals Inc., Lawrenceville, GA, USA), L-glutamine, and antibiotics [24].

Transfection of cells with p16INK4A plasmid

Target cells were grown in 6 well plates to a concentration of 1×10^6 cells/ml. These cells were untransfected, transfected with the empty vector (pCDNA3.1), or transfected with p16INK4A/pCNDA3.1 (encoding the full length p16INK4A gene) [25] with Gene Jammer (Stratagene, La Jolla, CA) as per the manufacturer's recommendations. After 48h post transfection, these cells (transiently transfected) were used in other experiments to analyze the role of p16INK4A in regulating KSHV reactivation.

Quantitative real-time PCR (qRT-PCR)

Total RNA was isolated using a Nucleospin RNA II kit (Clontech, Palo Alto, CA) as per manufacturer's recommendations. The cDNA was synthesized from the total RNA (500 ng) using the First-Strand cDNA Synthesis System (Invitrogen, Carlsbad, CA). The qRT-PCR was performed using the synthesized cDNA in single wells of a 96-well plate (BioRad, Hercules, CA) in a 25 μl reaction volume to analyze the expression of TK1 and β-actin transcripts as per earlier protocols using specific primers [26,27]. The thermocycling program consisted of 95° C for 3 min, followed by 40 cycles of 95°C for 15 sec and 60°C for 45 sec. The specificity and purity of the amplification reaction was determined by performing a melting curve analysis.

Western blotting

All the buffers used in this project were made with water that was endotoxin and pyrogen free. Equal amounts (25μg) of protein was used in Western blotting experiments [26]. The Western blots were routinely probed first with mouse anti-p16INK4A antibody (Clone ZJ11; Chemicon International, Temecula, CA). These blots were then "stripped' for reprobing with mouse anti-actin antibodies (Clone AC-74; Sigma) as per standard protocols [28].

Immunofluorescence assay (IFA)

Target cells were washed twice in phosphate buffered saline (PBS), spotted on glass slides, air-dried, and then fixed in ice-cold acetone for 10 min. The fixed cells were washed in PBS and stained sequentially with rabbit anti-gB antibodies [29] and goat anti-rabbit fluorescein isothiocyanate (FITC)-labelled secondary antibody (KPL, Gaithersburg, MD) for 30 min at 37°C. Stained cells were washed with PBS and were further incubated for 20 min at room temperature with 5 mM SYTO Red (a nuclear stain; Invitrogen) before being washed again and examined under a fluorescent microscope (Nikon Eclipse E600) with appropriate filters. In another set of experiments, acetone fixed target cells were stained simultaneously for the expression of KSHV gB and LANA with rabbit anti-gB antibodies and monoclonal antibodies to LANA (ABI, Columbia, MD), respectively. These cells were further incubated for 30 min with TRITC conjugated goat anti-rabbit antibodies and FITC conjugated goat anti-mouse antibodies as per procedures outlined above before being analyzed under a fluorescent microscope. The mean number of positive cells counted over five random fields was used for comparison and analysis. Arrowheads indicate cells that are positive for gB expression.

Synchronizing cells in different phases of cell cycle

We synchronized BCBL-1 and BCP-1 cells in G0/1 and S phase of cell cycle as per standard protocols [27,30]. Briefly, cells were synchronized at G0/1 by 24h of incubation in serum-free RPMI 1640 medium supplemented with antibiotics and 2 mM glutamine. Cells were synchronized at S phase of cell cycle by culturing the above (those synchronized in G0/1 phase) cells in RPMI 1640 medium supplemented with 10% FBS, antibiotics and 2 mM glutamine for 16h.

Flow cytometry

Flow cytometer was used to analyze cells in different stages of cell cycle. A 10 μg/ml concentration of Hoechst dye 33342 (Sigma) was added to the target cell suspension and incubated further at 37°C for 45 min. These cells were analyzed by FACScan flow cytometer (Becton Dickinson, San Jose, CA) to discriminate cells in different stages of cell cycle as per earlier protocols [28]. For another experiment, cells in S phase were treated with 20 ng/ml of TPA. After 36h post TPA treatment, these cells were washed twice in cold PBS and stained with rabbit anti-gB antibodies for 30min on ice. The cells were washed thrice in cold PBS and further incubated with a predetermined concentration of anti-rabbit antibodies conjugated to fluorescence isothiocyanate (FITC) (Sigma). After 30 min of incubation, these cells were washed as before and sorted for cells expressing gB on their surface using a FACScan flow cytometer (Becton Dickinson) as per standard lab protocols [28]. These gB positive sorted cells were washed twice in growth medium and further incubated for another 4h at 37°C before being analyzed by Raman tweezers.

Trypan blue test

Target cell survival was measured by staining cells with trypan blue solution (Sigma, St. Louis, MO) diluted to a final concentration of 0.04% (w/v). Stained cells were visualized using brightfield microscopy at 100× magnification. The number of viable (unstained) and non-viable (blue stained) cells were recorded as per standard procedure [31].

Analyzing cells by Raman tweezers

A detailed description of the Raman tweezers is provided in our earlier study [32]. Raman spectra for the different target cells were acquired using a spectrograph (Triax 320, Jobin Yvon Ltd, Edson, NJ) equipped with a liquid nitrogen cooled CCD detector. The Raman signal was collected in the spectral interval from 400 to 2100 cm^{-1} with a resolution of 6 cm^{-1}. Spectral acquisition for each cell was performed with a collection time of 60s, 20 mW at 780 nm. All the cells analyzed by this procedure were suspended in phenol red-free RPMI medium. Each individual cell was held in the laser beam and elevated from the cover slide about 10 μm to reduce the Brownian motion of the cell during the Raman acquisition and to reduce the fluorescence background from the glass cover slide. The Raman spectra of twenty cells were acquired for each cell type. Such single blinded studies were performed thrice on three different days. Fresh samples were used after acquisition of data for 10 cells. The background was recorded with the same acquisition conditions without trapping cells. Following spectral acquisition, the background signal originating from the cover slide and the surrounding medium was subtracted from all the spectra. The subtracted spectra were calibrated with the spectral response function of the Raman system.

RESULTS

Cell cycle is a determining factor for KSHV reactivation

KSHV reactivation is still an enigma. Recent studies demonstrated that the cells in S phase of cell cycle provide KSHV with the apt environment for a productive lytic cycle of infection or reactivation [28,30]. The above studies used cells sorted by flow cytometry [28] and serum starvation method [30] to arrive at the same conclusion. In this study we go a step further in that we analyzed the effect of endogenously over-expressing p16INK4A and analyzing its effect of KSHV reactivation. p16INK4A promotes G0/1 phase cell cycle arrest that is primarily dependent on a functional Rb protein [33]. KSHV infected BCBL-1 cells do not express p16INK4A [34]. BCBL-1 cells transfected with p16INK4A/pCNDA3.1 expressed elevated levels of p16INK4A when compared to cells transduced with empty vector (pCDNA3.1) (Fig. 1A). Untransfected cells did not express significant amounts of p16INK4A as observed by

Western blotting experiments (Fig. 1A). Cells transfected with p16INK4A/pCDNA3.1 resulted in an increase in the number of cells in G0/1 phase when compared to cells that were untransfected (Fig. 1B, C). Transfection of cells with the empty vector did not significantly alter the cell cycle progression (Fig. 1C). Next, we treated the above transfected cells with 20 ng/ml of TPA for 34h and analyzed for a possible reactivation of KSHV infection by monitoring gB (late lytic protein) by IFA. KSHV genome is maintained predominantly in a latent phase in BCBL-1 cells. Only 1–3% of cells spontaneously support lytic infection [35]. Expression of gB protein is an indicator of KSHV reactivation in BCBL-1 cells. Treatment of untransfected cells with TPA induced a significantly higher number of cells that supported a lytic infection as observed by the expression of gB (Fig. 1D). Identical results were observed in cells that were transfected with empty vector and TPA induced (Fig. 1D). However, TPA treatment of cells transfected with p16INK4A/pCDNA3.1 significantly lowered the expression of gB (Fig. 1D, E). Interestingly, cells expressing p16INK4A stained positive for LANA (latency associated nuclear antigen) but negative for gB (data not shown). Taken together, our results clearly indicate that the cells in G0/1 phase are less permissive to lytic infection when compared to those in S phase. These results corroborate with the earlier findings that cell cycle plays a crucial role in determining KSHV reactivation [28,30]. Target cells in S phase support reactivation to a significantly greater level when compared to those in G0/1 phase.

Analysis of BCBL-1 cells from different phases of cell cycle by Raman spectroscopy

A population of cells can be broadly divided into three groups based on cell cycle as G0/1, S, and G2/M phases. BCBL-1 cells harbor KSHV predominantly in a latent form. A lytic cycle of KSHV infection is supported primarily by BCBL-1 cells in S phase. As a first step towards delineating KSHV reactivation, we planned to obtain the Raman spectra of BCBL-1 cells in S phase that are capable of supporting a lytic infection. Towards this, cells were sorted in different phases of cell cycle by the conventional approach of serum starving [36]. Briefly, the cells were arrested in G0/1 phase of cell cycle by serum starving them for 24h. These cells were further incubated with 10% FBS at 37°C. After 16h incubation, the cells were found to be predominantly in S phase of cell cycle [30,37]. This was also confirmed by monitoring the expression of thymidine kinase 1 (TK1) gene by qRT-PCR. TK1, a cell cycle-dependent enzyme involved in the synthesis of DNA, is histological marker for cell proliferation [38]. TK1 gene expression is highly elevated in cells that enter S phase of cell cycle (actively dividing) while it is limited or almost absent in G0/1 phase, quiescent cells [28,39,40]. As expected, TK1 gene expression was six fold higher in BCBL-1 cells obtained 16h post FBS treatment of serum starved cells (S phase of cell cycle) when compared to those obtained 24h after serum starvation (G0/1 phase) (Fig. 2A). No detectable signal was observed with reactions performed in the absence of template (data not shown), demonstrating the specificity of the qRT-PCR conducted.

Raman spectra were obtained for cells from three different groups: (1) cells in G0/1 phase, (2) cells in S phase, and (3) cells from S phase that were TPA induced for 48h. The basis for selecting these three groups is the inherent variation in the cellular environment among the three groups with respect to KSHV reactivation. The experimental set up for the Raman tweezers is described in the methods section. Each of these cells was trapped optically and analyzed using Raman tweezers. The cells have a rounded morphology with an average diameter of 8–12 μm. For each cell type, the Raman acquisition was done only for the nuclei portion of the cells with the confocal LTRS system. The Raman spectrum of BCBL-1 cells under physiological conditions was recorded at 22°C (Fig. 2B). Among the other subtle differences, the intensities of the Raman bands at 813 and 830 cm^{-1} were significantly altered in the nucleus of KSHV infected cells from S phase and TPA-induced cells from S phase when compared to cells from G0/1 phase (Fig. 2B, C). The intensities of the Raman bands at 813 cm^{-1} was significantly greater in cells from S phase when compared to those in cells from

G0/1 and TPA-induced cells from S phase (Fig. 2C). The 813 cm^{-1} band intensity was significantly lower in TPA-induced cells from S phase when compared to cells from G0/1 and S phase (Fig. 2C). On the same note, the intensity of band at 830 cm^{-1} was significantly greater in TPA-induced cells from S phase when compared to cells from G01 and S phase (Fig. 2C). The Raman spectra for S phase cells treated with DMSO (the vehicle for TPA) was comparable to the one obtained for the cells from S phase (data not shown). Interestingly, the band intensities of the peaks at 785 and 1660 cm^{-1} between the three groups of cells remained comparable demonstrating the specificity of the Raman signals.

TPA treatment of cells results in an induction of a lytic infection in BCBL-1 cells. By 48h post TPA induction, some cells start to show signs of death. In order to confirm that cells analyzed by Raman tweezers were very much viable and not dead, we did two things as follows: (1) analyzed percentage dead cells by trypan blue test; and (2) obtained Raman spectra of dead cells. Under our laboratory conditions, greater than 95% of cells were found to be viable in G0/1 and S phase (Fig. 3A). However, we determined 13±4% of cells to be dead in TPA-induced cells from S phase (Fig. 3A). Under a bright field microscope, dead cells appear to have lost membrane integrity. We acquired the Raman spectra for such dead cells and found one unique peak that was significantly greater in them when compared to the viable cells in G0/1, S, and TPA-induced cells from S phase (Fig. 3B). This was Raman band at 1050 cm^{-1} (Fig. 3B). Interestingly, this band was not observed at the same intensity in cells from G0/1, S, and TPA-induced cells from S phase (Fig. 3C). These results confirm the authenticity of our Raman bands for cells from G0/1, S, and TPA-induced cells from S phase. Taken together, Raman tweezers successfully identified the crucial fingerprints of cells that have the propensity to support a lytic infection (cells from S phase).

Analysis of PEL cells specifically supporting KSHV reactivation by Raman tweezers

TPA treatment of cells induces KSHV lytic infection. However, the analysis of TPA-induced cells from S phase does not quite provide the Raman bands that were specific to reactivation. This is partly because of the fact that TPA treatment of cells only induces reactivation in about 20–25% of the cells [35]. Hence, we attempted to obtain Raman spectra of flow cytometry sorted cells that were specifically undergoing reactivation. To authenticate our results, we used two different KSHV infected PEL cells in the following studies: BCBL-1 and BCP-1 cells [22].

The goal was achieved by analyzing the flow cytometry sorted cells that were specifically undergoing reactivation by Raman tweezers as per protocols outlined in the schematic line drawing (Fig. 4A). The key was to sort cells expressing gB, an envelope associated protein termed as a “late protein” which is a classic indicator of a lytic infection [35]. Forward- and side-scatter plot was used to gate the population of BCBL-1 (Fig. 4B) and BCP-1 cells (data not shown) for sorting. We observed 20–25% of TPA-induced cells from S phase to express gB in BCBL-1 cells (Fig. 4C, D). Identical results were observed in TPA-induced BCP-1 cells (data not shown). These results were further confirmed by IFA using rabbit anti-gB antibodies (Fig. 4E). The results from IFA studies corroborate the findings from FACs analysis.

Cells from S phase that were TPA-induced were screened in a flow cytometer, sorted based on the expression of gB, and were analyzed by Raman tweezers. Cells that were gB positive supported a KSHV lytic infection (reactivation) while, cells that were gB negative supported a latent infection. All the cells analyzed by Raman tweezers were live and not dead. This is also apparent by the absence of a strong Raman band at 1050 cm^{-1} (Fig. 5A, B). PEL cells supporting KSHV reactivation had weak and strong bands at 813 and 830 cm^{-1}, respectively (Fig. 5A, B). In addition, there were three other peaks that were unique to cells supporting KSHV reactivation when compared to cells supporting a latent infection. PEL cells supporting virus reactivation had weak bands at 785 and 1095 cm^{-1}; and a stronger band at 1128 cm^{-1}

when compared to cells supporting a latent infection (Fig. 5A, B). Taken together, for the first time unique fingerprints of cells supporting KSHV reactivation has been delineated.

DISCUSSION

There are several viruses that produce latent infection in target cells. These viruses have a specific phase during their replication cycle when a latent infection is terminated. Termination of latency leads to a lytic replication phase. As of this date, the exact mechanism behind this switch from latent to lytic infection is still elusive. Herein, we have attempted to use a combination of biochemical assays, molecular biology tools, and Raman tweezers to decipher the crucial signature of cells supporting virus reactivation; and in the process, we have used KSHV as a model to analyze this goal. Raman spectroscopy has been previously used to understand several aspects of biology such as different stages of virus infection, biology of cancers, and so on [32,41–43].

TPA treatment of PEL cells transfected with p16INK4A/pCDNA3.1 did not significantly enhance lytic infection when compared to the untransfected cells (Fig. 1). The results from these transfection experiments supported the fact that the cells from S phase provide the optimal conditions for KSHV reactivation. These results support earlier findings by others and us [28,30]. Hence, we acquired Raman specific bands for cells in G0/1, S, and S phase cells treated with TPA. The spectra of all the cell types used in this study share many similar peaks that can be assigned to cellular constituents: nucleic acids (DNA/RNA), proteins, lipids, and carbohydrates. The two major peaks that were found to be significantly altered between cells from G0/1, S, and cells from S phase that were TPA treated were at 813 and 830 cm^{-1} (Fig. 2B, C). The Raman band at 813 cm^{-1} denotes the RNA concentration within the nucleus [44]. The cells in S phase are significantly active when compared to the quiescent cells from G0/1 phase (Fig. 2A). This means the level of transcription occurring within the nucleus is elevated during S phase when compared to G0/1 phase resulting in more of RNA accumulation. Accordingly, the Raman band at 813 cm^{-1} is stronger in S phase when compared to G0/1 phase (Fig. 2C). However, the peak at 813 cm^{-1} is specifically and significantly weak in TPA-induced cells from S phase (Fig. 2C). This could be due to one or both of the following reasons: (1) A significant population of cells in S phase would be supporting a lytic infection. At this stage, the cellular machinery is overwhelmed by active KSHV replication and virus-induced host transcription shutoff; both of which may eventually result in cell death. Of these, the KSHV-induced host transcription shutoff specifically results in host cell RNA degradation and thus a weak 813cm^{-1} band [27,45]; and (2) it is a reflection of a complicated set of events occurring within the cells during reactivation. The peak at 830 cm^{-1} represents tyrosine side chains and vibrations in the adenine, thymine 1, and thymine 2 sugars [46,47]. Tyrosine is a unique amino acid that can be specifically phosphorylated by kinases crucial in the transduction of signals from within the nucleus to the outside and *vice versa*; while adenine and thymine are the components of DNA. This peak is specifically stronger only in TPA-induced cells from S phase when compared to cells from G0/1 and S phases. This makes sense as TPA induces not only cell proliferation but also reactivation of virus infection. These results proved the point that Raman tweezers can distinguish between cells from G0/1, S, and TPA-induced cells from S phase. In other words, Raman tweezers efficiently deciphered the fingerprints of cells (cells in S phase) that had the propensity to support KSHV reactivation. However, this approach could not identify the fingerprints of the cells actually supporting reactivation because TPA induced reactivation of only 20–25% of cells in S phase (Fig. 4D, E).

In order to specifically delineate the Raman spectra of cells supporting KSHV reactivation, we followed a novel approach where cells were sorted based on the state of infection (latent Vs lytic) by a flow cytometer and then analyzed by the Raman tweezers. The state of infection was determined by the expression of the KSHV lytic protein (gB) on the cell surface. KSHV

gB is expressed on the surface of cells supporting a lytic infection [29]. In order to screen only cells that were supporting KSHV reactivation, we incubated the cells in growth medium after sorting them through the flow cytometer. This additional step of incubation for 4h was done for two reasons: (1) eliminate any further effect of TPA, and (2) equilibrate cells from the effect of staining procedure. The cells supporting KSHV reactivation had a weaker band at 813 cm^{-1} and a stronger band at 830 cm^{-1} when compared to cells that were supporting a latent KSHV infection (Fig. 5B). This data was comparable to what was observed for TPA-induced cells from S phase (Fig. 2C). The Raman bands at 785 cm^{-1} and 1095 cm^{-1} for cells supporting KSHV reactivation were significantly weak when compared to cells that were supporting a latent infection (Fig. 5B). Apart from this, the Raman band at 1128 cm^{-1} was significantly strong in cells supporting KSHV reactivation when compared to cells supporting a latent infection (Fig. 5B). The 785 cm^{-1}, 1095 cm^{-1}, and 1128 cm^{-1} Raman bands indicate the phosphodiester bond C'_5-O-P-O-C'_3 and pyrimidine nucleobases; phosphodioxy groups PO_2^- of the DNA backbone; and vibrations of C-N in proteins and C-C in lipids, respectively [48–50].

To understand the physiological relevance of these peaks to KSHV reactivation, one has to understand the virus lytic infection. Like other herpesviruses, KSHV lytic infection is characterized by immediate shut off of the host RNA and DNA synthesis [51]. Herpesviruses are said to alter the host cell macromolecular metabolism by at least 4 manners: (1) host cell mRNA is degraded, (2) transcription is shut off, (3) cellular proteins are degraded, and (4) cellular proteins are redirected to perform function that directly benefit the lytic replication. All of the above cellular changes allow virus to replicate successfully, produce progeny virions, and finally kill the cells. These cellular changes are reflected in the Raman bands (Table 1) in that the RNA (813 cm^{-1}) and DNA (785 cm^{-1} and 1095 cm^{-1}) levels are lower in cells supporting KSHV reactivation. It feels as if the Raman band specific for DNA (1095 cm^{-1}) should have been stronger than what is observed based on the fact that the virus is actively replicating. This data on the peak 1095 cm^{-1}, we believe, is a strong reflection what is occurring within the infected cell during the late stages of lytic infection. Late stage of infection is classified based on the temporal expression of the KSHV encoded secondary late lytic gene (ORF 8 that encodes for gB, a structural protein). Genes involved in KSHV DNA replication are detected at significant levels during very early stages (by 14 to 20h post lytic infection). They primarily aid in DNA repair and nucleotide metabolism. On the contrary, proteins and lipids that form part of KSHV (tegument, capsid, and envelope associated glycoproteins) are expressed very late during virus life cycle (about 34h and later) [52]. This late spike in the viral proteins and lipids could be the result of strong Raman bands at 830 cm^{-1} and 1128 cm^{-1}. All these 5 peaks seem to make up the distinct Raman fingerprints of the cells supporting KSHV reactivation.

Taken together, the results reported here describe the first use of a combination of molecular biology, biochemical assays, and Raman tweezers in analyzing the cellular events required to support a KSHV reactivation. This method will prove useful in the future to decipher the critical cellular events that trigger reactivation of KSHV latency. To date, all of the antivirals used to treat herpesvirus infections target only the lytic state of infection. Hence, these antivirals can never get rid of the virus completely. Understanding the molecular switch vital for the reactivation of latent infections will definitely open the door for developing new strategies capable of controlling, and perhaps eradicating, latent viral infections. We are certain that the present findings will serve as a model to unravel the mysteries surrounding virus latency.

Acknowledgments

This work was supported in part by NIH/NIBIB grant R21EB006483. We also thank Mr. Huxley for critically reading this manuscript.

References

1. Chang Y, Cesarman E, Pessin MS, Lee F, Culpepper J, Knowles DM, Moore PS. Identification of herpesvirus-like DNA sequences in AIDS-associated Kaposi's sarcoma. Science 1994;266:1865–1869. [PubMed: 7997879]
2. Hamden KE, Whitman AG, Ford PW, Shelton JG, McCubrey JA, Akula SM. Raf and VEGF: emerging therapeutic targets in Kaposi's sarcoma-associated herpesvirus infection and angiogenesis in hematopoietic and nonhematopoietic tumors. Leukemia 2005;19:18–26. [PubMed: 15470486]
3. Ganem D. Human herpesvirus 8 and its role in the genesis of Kaposi's sarcoma. Curr Clin Top Infect Dis 1998;18:237–251. [PubMed: 9779358]
4. Ensoli B, Sgadari C, Barillari G, Sirianni MC, Sturzl M, Monini P. Biology of Kaposi's sarcoma. Eur J Cancer 2001;37:1251–1269. [PubMed: 11423257]
5. Grundhoff A, Ganem D. Inefficient establishment of KSHV latency suggests an additional role for continued lytic replication in Kaposi sarcoma pathogenesis. J Clin Invest 2004;113:124–136. [PubMed: 14702116]
6. Wang CY, Sugden B. New viruses shake old paradigms. J Clin Invest 2004;113:21–23. [PubMed: 14702103]
7. Dezube BJ, Zambela M, Sage DR, Wang JF, Fingeroth JD. Characterization of Kaposi sarcoma-associated herpesvirus/human herpesvirus-8 infection of human vascular endothelial cells: early events. Blood 2002;100:888–896. [PubMed: 12130499]
8. Blasig C, Zietz C, Haar B, Neipel F, Esser S, Brockmeyer NH, Tschachler E, Colombini S, Ensoli B, Sturzl M. Monocytes in Kaposi's sarcoma lesions are productively infected by human herpesvirus 8. J Virol 1997;71:7963–7968. [PubMed: 9311888]
9. Diamond C, Brodie SJ, Krieger JN, Huang ML, Koelle DM, Diem K, Muthui D, Corey L. Human herpesvirus 8 in the prostate glands of men with Kaposi's sarcoma. J Virol 1998;72:6223–6227. [PubMed: 9621094]
10. Staskus KA, Zhong W, Gebhard K, Herndier B, Wang H, Renne R, Beneke J, Pudney J, Anderson DJ, Ganem D, Haase A. Kaposi's sarcoma-associated herpesvirus gene expression in endothelial (spindle) tumor cells. J Virol 1997;71:715–719. [PubMed: 8985403]
11. Whitby D, Howard MR, Tenant-Flowers M, Brink NS, Copas A, Boshoff C, Hatzioannou T, Suggett FE, Aldam DM, Denton AS, et al. Detection of Kaposi sarcoma associated herpesvirus in peripheral blood of HIV-infected individuals and progression to Kaposi's sarcoma. Lancet 1995;346:799–802. [PubMed: 7674745]
12. Medveczky MM, Horvath E, Lund T, Medveczky PG. In vitro antiviral drug sensitivity of the Kaposi's sarcoma-associated herpesvirus. Aids 1997;11:1327–1332. [PubMed: 9302441]
13. Renne R, Zhong W, Herndier B, McGrath M, Abbey N, Kedes D, Ganem D. Lytic growth of Kaposi's sarcoma-associated herpesvirus (human herpesvirus 8) in culture. Nat Med 1996;2:342–346. [PubMed: 8612236]
14. Jordan MC, Jordan GW, Stevens JG, Miller G. Latent herpesviruses of humans. Ann Intern Med 1984;100:866–880. [PubMed: 6326635]
15. Seiler P, Senn BM, Klenerman P, Kalinke U, Hengartner H, Zinkernagel RM. Additive effect of neutralizing antibody and antiviral drug treatment in preventing virus escape and persistence. J Virol 2000;74:5896–5901. [PubMed: 10846070]
16. Duca KA, Shapiro M, Delgado-Eckert E, Hadinoto V, Jarrah AS, Laubenbacher R, Lee K, Luzuriaga K, Polys NF, Thorley-Lawson DA. A virtual look at Epstein-Barr virus infection: biological interpretations. PLoS Pathog 2007;3:1388–1400. [PubMed: 17953479]
17. Cook SD, Paveloff MJ, Doucet JJ, Cottingham AJ, Sedarati F, Hill JM. Ocular herpes simplex virus reactivation in mice latently infected with latency-associated transcript mutants. Invest Ophthalmol Vis Sci 1991;32:1558–1561. [PubMed: 1849874]
18. Cesarman E. The role of Kaposi's sarcoma-associated herpesvirus (KSHV/HHV-8) in lymphoproliferative diseases. Recent Results Cancer Res 2002;159:27–37. [PubMed: 11785841]
19. Glaser R, Kiecolt-Glaser JK, Speicher CE, Holliday JE. Stress, loneliness, and changes in herpesvirus latency. J Behav Med 1985;8:249–260. [PubMed: 3003360]

20. Xie C, Mace J, Dinno MA, Li YQ, Tang W, Newton RJ, Gemperline PJ. Identification of single bacterial cells in aqueous solution using confocal laser tweezers Raman spectroscopy. Anal Chem 2005;77:4390–4397. [PubMed: 16013851]
21. Lambert PJ, Whitman AG, Dyson OF, Akula SM. Raman spectroscopy: the gateway into tomorrow's virology. Virol J 2006;3:51. [PubMed: 16805914]
22. Akula SM, Ford PW, Whitman AG, Hamden KE, Bryan BA, Cook PP, McCubrey JA. B-Raf-dependent expression of vascular endothelial growth factor-A in Kaposi sarcoma-associated herpesvirus-infected human B cells. Blood 2005;105:4516–4522. [PubMed: 15705790]
23. Ramser K, Bjerneld EJ, Fant C, Kall M. Importance of substrate and photo-induced effects in Raman spectroscopy of single functional erythrocytes. J Biomed Opt 2003;8:173–178. [PubMed: 12683842]
24. Akula SM, Ford PW, Whitman AG, Hamden KE, Shelton JG, McCubrey JA. Raf promotes human herpesvirus-8 (HHV-8/KSHV) infection. Oncogene 2004;23:5227–5241. [PubMed: 15122343]
25. Medema RH, Herrera RE, Lam F, Weinberg RA. Growth suppression by p16ink4 requires functional retinoblastoma protein. Proc Natl Acad Sci U S A 1995;92:6289–6293. [PubMed: 7603984]
26. Dyson OF, Bryan BA, Lambert PJ, Ford PW, Akula SM. beta1 Integrins Mediate Tubule Formation Induced by Supernatants Derived from KSHV-Infected Cells. Intervirology 2007;50:245–253. [PubMed: 17460413]
27. Whitman AG, Dyson OF, Lambert PJ, Oxendine TL, Ford PW, Akula SM. Changes occurring on the cell surface during KSHV reactivation. J Electron Microsc (Tokyo) 2007;56:27–36. [PubMed: 17392397]
28. Bryan BA, Dyson OF, Akula SM. Identifying cellular genes crucial for the reactivation of Kaposi's sarcoma-associated herpesvirus latency. J Gen Virol 2006;87:519–529. [PubMed: 16476973]
29. Akula SM, Pramod NP, Wang FZ, Chandran B. Human herpesvirus 8 envelope-associated glycoprotein B interacts with heparan sulfate-like moieties. Virology 2001;284:235–249. [PubMed: 11384223]
30. McAllister SC, Hansen SG, Messaoudi I, Nikolich-Zugich J, Moses AV. Increased efficiency of phorbol ester-induced lytic reactivation of Kaposi's sarcoma-associated herpesvirus during S phase. J Virol 2005;79:2626–2630. [PubMed: 15681463]
31. Shaw AM, Braun L, Frew T, Hurley DJ, Rowland RR, Chase CC. A role for bovine herpesvirus 1 (BHV-1) glycoprotein E (gE) tyrosine phosphorylation in replication of BHV-1 wild-type virus but not BHV-1 gE deletion mutant virus. Virology 2000;268:159–166. [PubMed: 10683338]
32. Hamden KE, Bryan BA, Ford PW, Xie C, Li YQ, Akula SM. Spectroscopic analysis of Kaposi's sarcoma-associated herpesvirus infected cells by Raman tweezers. J Virol Methods 2005;129:145–151. [PubMed: 15992938]
33. Lukas J, Aagaard L, Strauss M, Bartek J. Oncogenic aberrations of p16INK4/CDKN2 and cyclin D1 cooperate to deregulate G1 control. Cancer Res 1995;55:4818–4823. [PubMed: 7585513]
34. Platt G, Carbone A, Mittnacht S. p16INK4a loss and sensitivity in KSHV associated primary effusion lymphoma. Oncogene 2002;21:1823–1831. [PubMed: 11896614]
35. Ford PW, Bryan BA, Dyson OF, Weidner DA, Chintalgattu V, Akula SM. Raf/MEK/ERK signalling triggers reactivation of Kaposi's sarcoma-associated herpesvirus latency. J Gen Virol 2006;87:1139–1144. [PubMed: 16603514]
36. Krek W, DeCaprio JA. Cell synchronization. Methods Enzymol 1995;254:114–124. [PubMed: 8531680]
37. Hinz M, Krappmann D, Eichten A, Heder A, Scheidereit C, Strauss M. NF-kappaB function in growth control: regulation of cyclin D1 expression and G0/G1-to-S-phase transition. Mol Cell Biol 1999;19:2690–2698. [PubMed: 10082535]
38. Mao Y, Wu J, Skog S, Eriksson S, Zhao Y, Zhou J, He Q. Expression of cell proliferating genes in patients with non-small cell lung cancer by immunohistochemistry and cDNA profiling. Oncol Rep 2005;13:837–846. [PubMed: 15809747]
39. Ohrvik A, Lindh M, Einarsson R, Grassi J, Eriksson S. Sensitive nonradiometric method for determining thymidine kinase 1 activity. Clin Chem 2004;50:1597–1606. [PubMed: 15247154]
40. Gross MK, Merrill GF. Thymidine kinase synthesis is repressed in nonreplicating muscle cells by a translational mechanism that does not affect the polysomal distribution of thymidine kinase mRNA. Proc Natl Acad Sci U S A 1989;86:4987–4991. [PubMed: 2740335]

41. Jess PR, Smith DD, Mazilu M, Dholakia K, Riches AC, Herrington CS. Early detection of cervical neoplasia by Raman spectroscopy. Int J Cancer 2007;121:2723–2728. [PubMed: 17724716]

42. Sun Y, Overman SA, Thomas GJ Jr. Impact of in vitro assembly defects on in vivo function of the phage P22 portal. Virology 2007;365:336–345. [PubMed: 17490703]

43. Raso SW, Clark PL, Haase-Pettingell C, King J, Thomas GJ Jr. Distinct cysteine sulfhydryl environments detected by analysis of Raman S-hh markers of Cys-->Ser mutant proteins. J Mol Biol 2001;307:899–911. [PubMed: 11273709]

44. Uzunbajakava N, Lenferink A, Kraan Y, Volokhina E, Vrensen G, Greve J, Otto C. Nonresonant confocal Raman imaging of DNA and protein distribution in apoptotic cells. Biophys J 2003;84:3968–3981. [PubMed: 12770902]

45. Glaunsinger B, Ganem D. Lytic KSHV infection inhibits host gene expression by accelerating global mRNA turnover. Mol Cell 2004;13:713–723. [PubMed: 15023341]

46. Meng G, Chan JC, Rousseau D, Li-Chan EC. Study of protein-lipid interactions at the bovine serum albumin/oil interface by Raman microspectroscopy. J Agric Food Chem 2005;53:845–852. [PubMed: 15712988]

47. Dadarlat VM, Saxena VK. Stability of triple-helical poly(dT)-poly(dA)-poly(dT) DNA with counterions. Biophys J 1998;75:70–91. [PubMed: 9649369]

48. Borchman D, Tang D, Yappert MC. Lipid composition, membrane structure relationships in lens and muscle sarcoplasmic reticulum membranes. Biospectroscopy 1999;5:151–167. [PubMed: 10380082]

49. Notingher I, Verrier S, Haque S, Polak JM, Hench LL. Spectroscopic study of human lung epithelial cells (A549) in culture: living cells versus dead cells. Biopolymers 2003;72:230–240. [PubMed: 12833477]

50. Chan JW, Taylor DS, Zwerdling T, Lane SM, Ihara K, Huser T. Micro-Raman spectroscopy detects individual neoplastic and normal hematopoietic cells. Biophys J 2006;90:648–656. [PubMed: 16239327]

51. Chandriani S, Ganem D. Host transcript accumulation during lytic KSHV infection reveals several classes of host responses. PLoS ONE 2007;2:e811. [PubMed: 17726541]

52. Jenner RG, Alba MM, Boshoff C, Kellam P. Kaposi's sarcoma-associated herpesvirus latent and lytic gene expression as revealed by DNA arrays. J Virol 2001;75:891–902. [PubMed: 11134302]

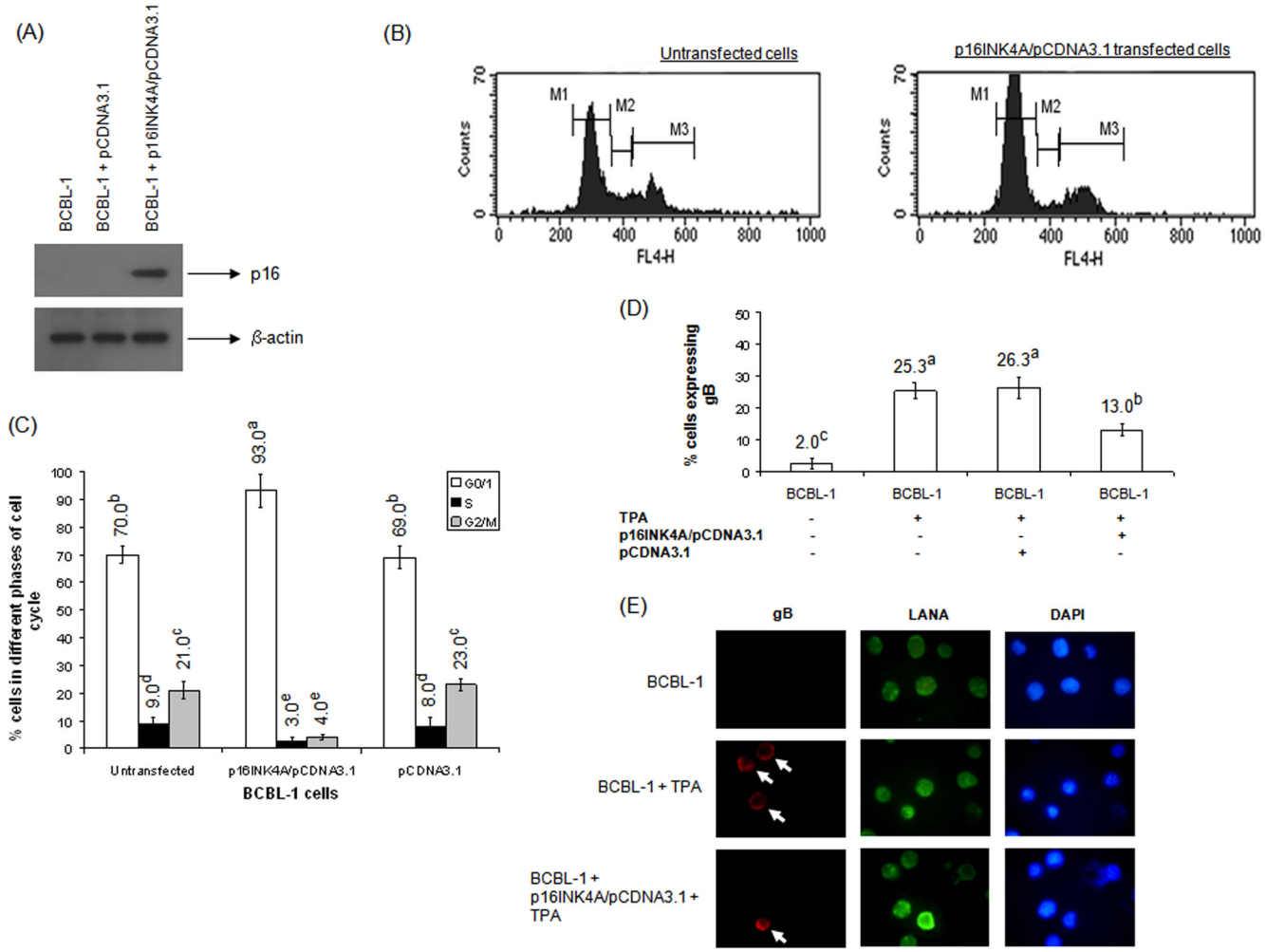

Figure 1. Ectopic expression of p16INK4A induces cell cycle arrest in G0/1 phase resulting in a decreased response to TPA-induced reactivation

(A) BCBL-1 cells were untransfected, transfected with empty vector (pCDNA3.1), or p16INK4A/pCDNA3.1. Western blot analysis of p16INK4A and β-actin expression in the above cells was performed at 48 h post transfection. The bands were scanned and the band intensities were assessed using the ImageQuaNT software program (Molecular Dynamics). **(B)** Flow cytometer was used to analyze cell cycle in target cells. Representative histograms depicting cell cycle in untransfected and p16INK4A/pCDNA3.1 transfected BCBL-1 cells stained with Hoechst dye 33342 is shown. **(C)** The % number of cells in different phases of cell cycle is provided based on the results from three different trials. Data presented represent the average ± SD of three experiments. Average values on the columns with different superscripts are statistically significant ($P<0.05$) by least significant difference (LSD). **(D)** IFA was performed to analyze the expression of gB in the above cells. The percentage cells expressing gB under different conditions is provided. Data presented represent the average ± SD of three experiments. Average values on the columns with different superscripts are statistically significant ($P<0.05$) by LSD. Representative images of IFA experimentation is provided for reference **(E)**. Magnification: 100X.

(A)

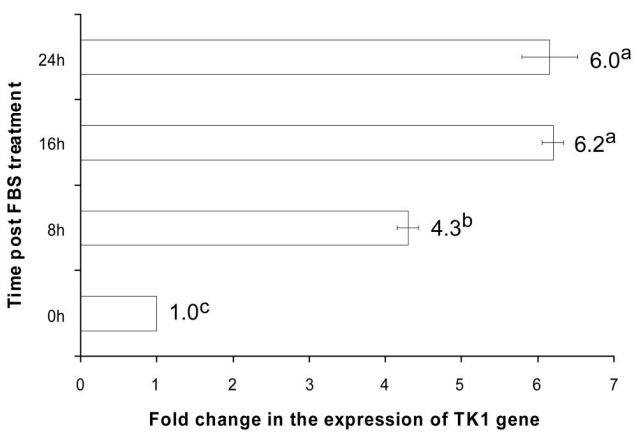

(B)

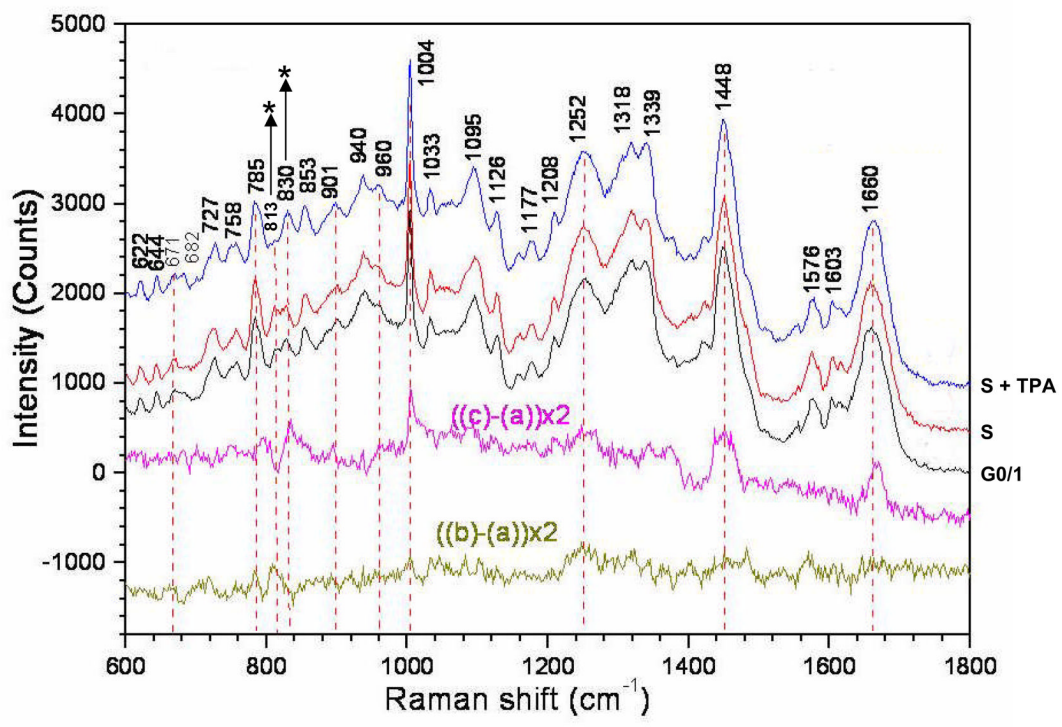

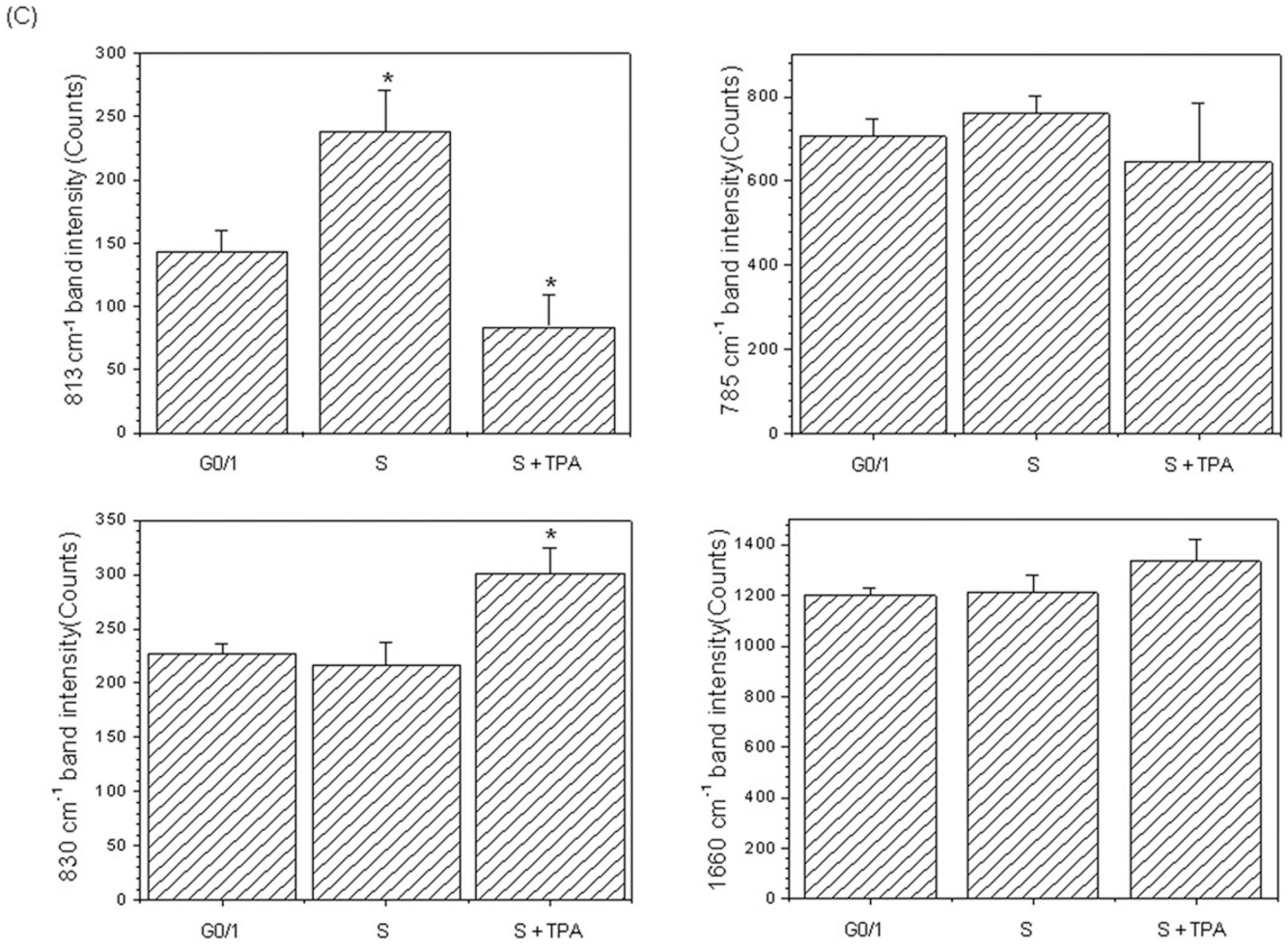

Figure 2.

(A) BCBL-1 cells in S phase express elevated levels of TK1. BCBL-1 cells were serum starved for 24h. These cells were incubated in RPMI containing 10% FBS. The cells were collected at 0, 8, 16, and 24h post FBS addition, lysed, RNA extracted, and qRT-PCR performed as per standard protocols. The fold increase in the expression of TK1 gene expression is represented in histogram and was calculated based on the standard graph generated by qRT-PCR of a known concentration of the TK1 gene. Expression of TK1 gene at 0h was considered as 1 fold. The lowest limit of detection in the standard samples was 6 to 60 copies for the TK1 gene. The data presented in the histogram was from three independent experiments. Average values on columns with different superscripts are statistically significant (P<0.05) by LSD. **(B) Raman spectra of BCBL-1 cells from different stages of cell cycle**. Average Raman spectra of individual BCBL-1 cells from G0/1, S, and S phase induced with TPA in the fingerprint range from 600 cm^{-1} to 1800 cm^{-1} is depicted. Raman bands that occur between BCBL-1 cells obtained from G0/1 (a), S (b), and S phase cells that were induced with TPA (c) is shown. Each spectrum was obtained by averaging the spectra of 20 individual cells. **(C)** Spectral changes in 785 cm^{-1}, 813 cm^{-1}, 830 cm^{-1}, and 1660 cm^{-1} bands are shown. The spectra are an average of data from 20 cells. Average values on columns with different superscripts are statistically significant (P<0.05) by LSD.

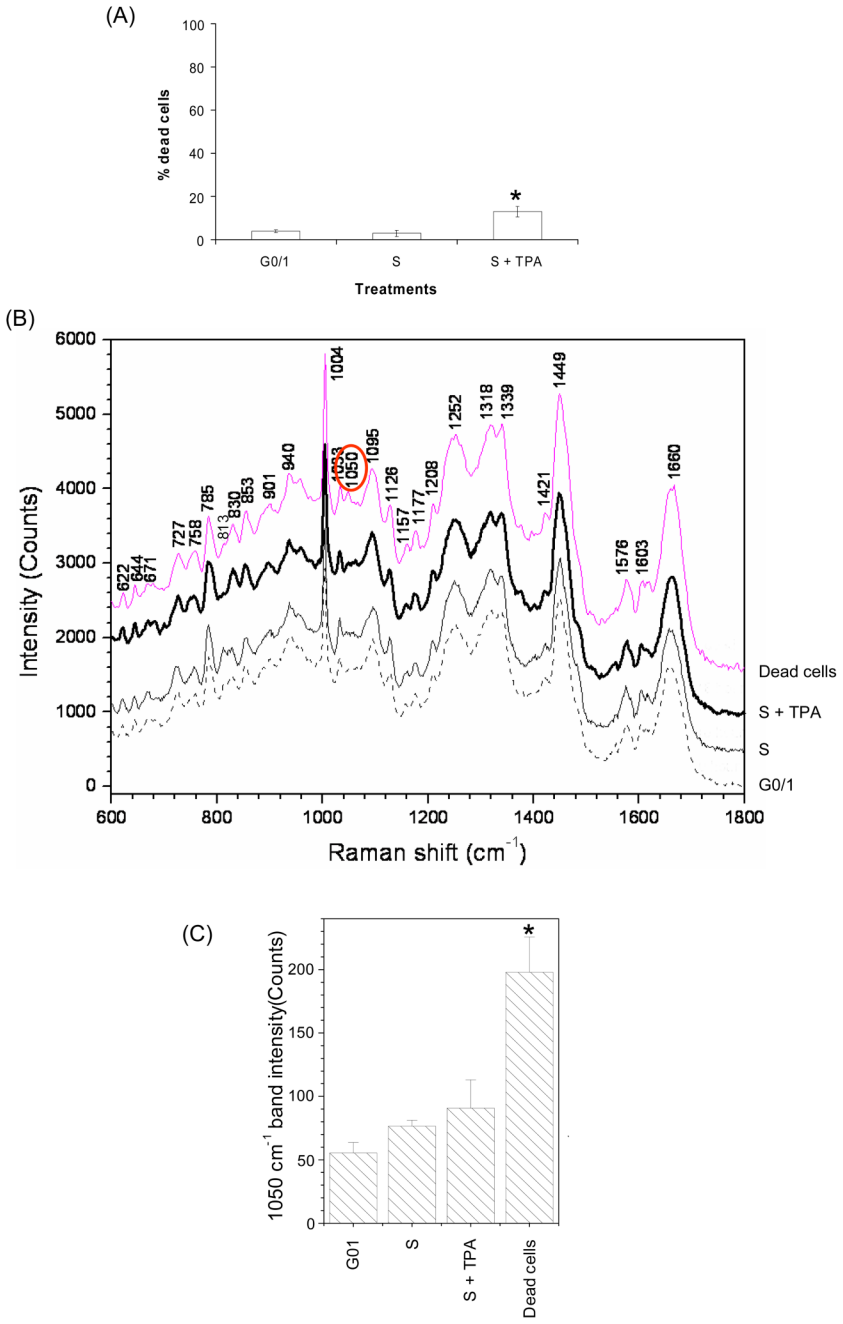

Figure 3. Dead BCBL-1 cells have a distinct Raman band at 1050 cm^{-1}

(A) Data from trypan blue test to monitor % dead cells is shown. Data presented represent the average ± SD of three experiments. The column with an asterisk mark indicates the value to be statistically significant (P<0.05) by LSD. **(B)** Comparing Raman spectra of dead cells with the cells obtained from G0/1, S, and TPA-induced S phase cells. Each spectrum was obtained by averaging the spectra of 20 individual cells. The Raman band at 1050 cm^{-1} is circled. **(C)** Spectral changes in 1050 cm^{-1} Raman band that occur between BCBL-1 cells obtained from G0/1, S, S phase cells that were induced with TPA, and dead cells is shown. The spectra are an average of data from 20 cells. The column with an asterisk mark indicates the value to be statistically significant (P<0.05) by LSD.

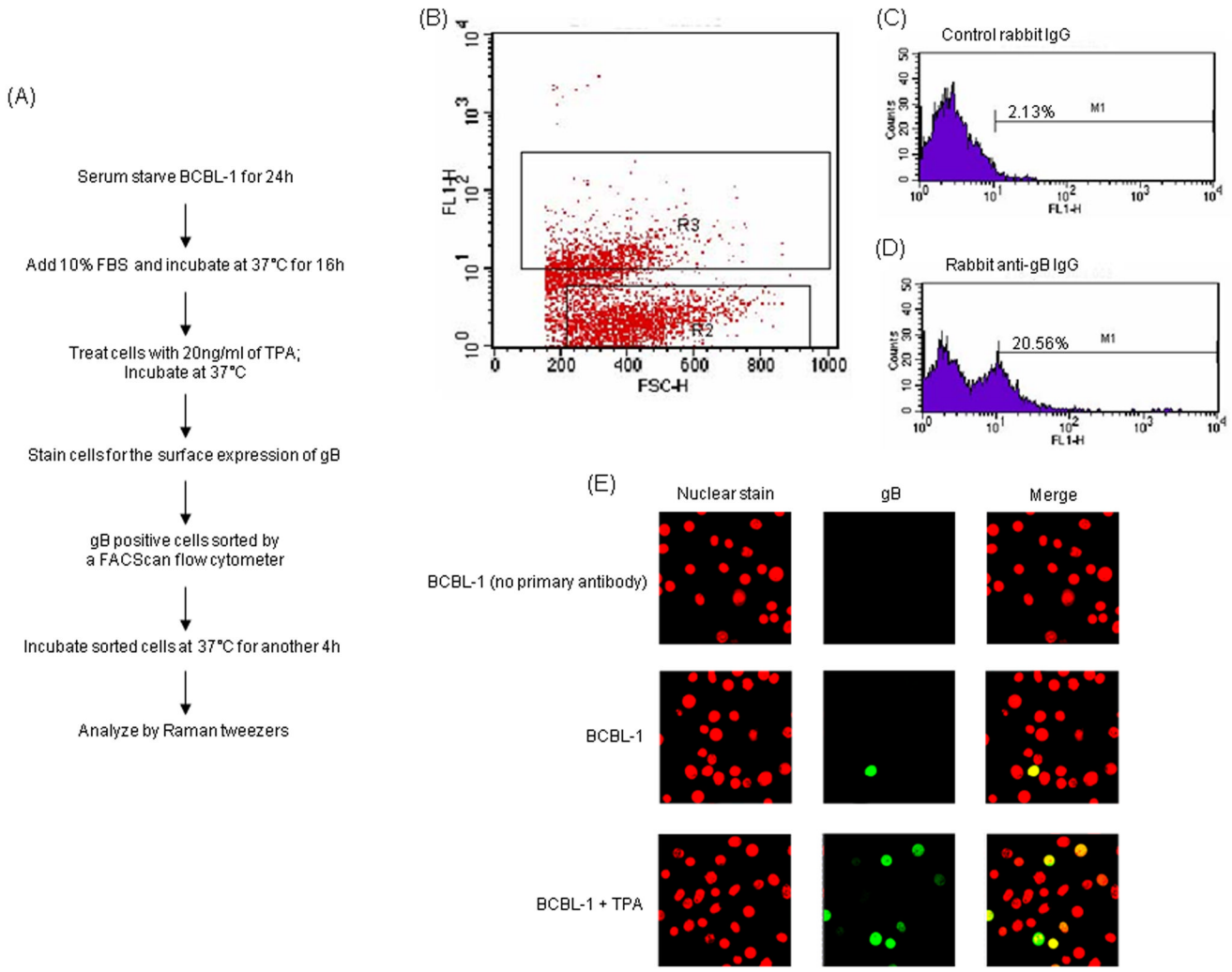

Figure 4. Flow cytometer was used to sort cells that were actively supporting KSHV reactivation

(A) Schematic line drawing showing the experimental protocol involved in assessing the fingerprint of BCBL-1 cells supporting KSHV reactivation. Cells in S phase were TPA treated for 36h. These cells were stained for the surface expression of gB and analyzed in a FACScan flow cytometer. **(B)** A representative forward- and side-scatter plot of these stained cells is provided. **(C, D)** Cells in R3 were sorted to obtain cells that were negative and positive for surface gB expression. **(E)** These sorted cells were incubated sequentially with rabbit polyclonal antibodies to gB and FITC–anti-rabbit antibodies. Finally, the stained cells were further incubated for 20 min on ice with 5 mM SYTO Red (a nuclear stain; Invitrogen) and examined under a fluorescent microscope using respective filters. Magnification: 62x.

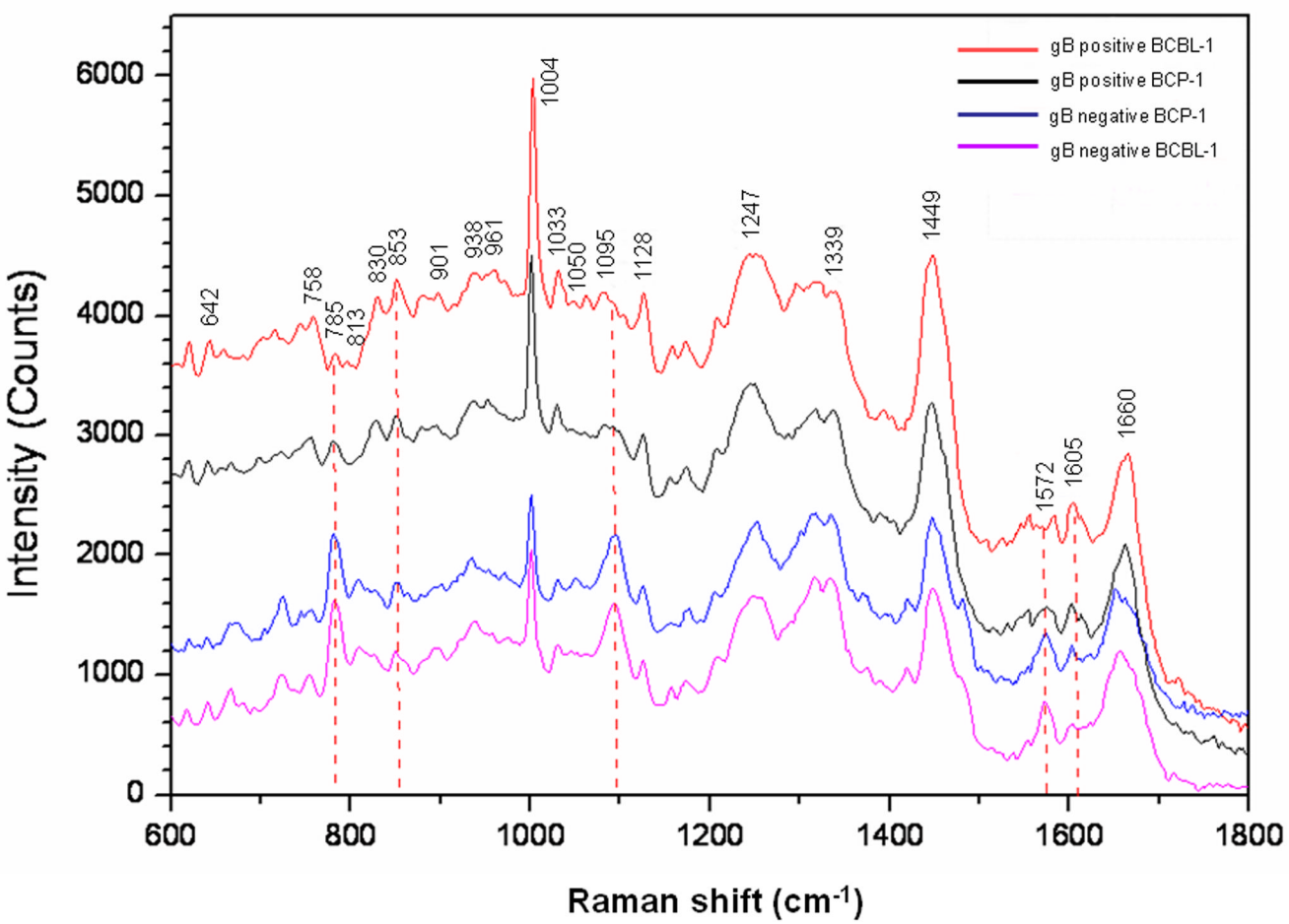

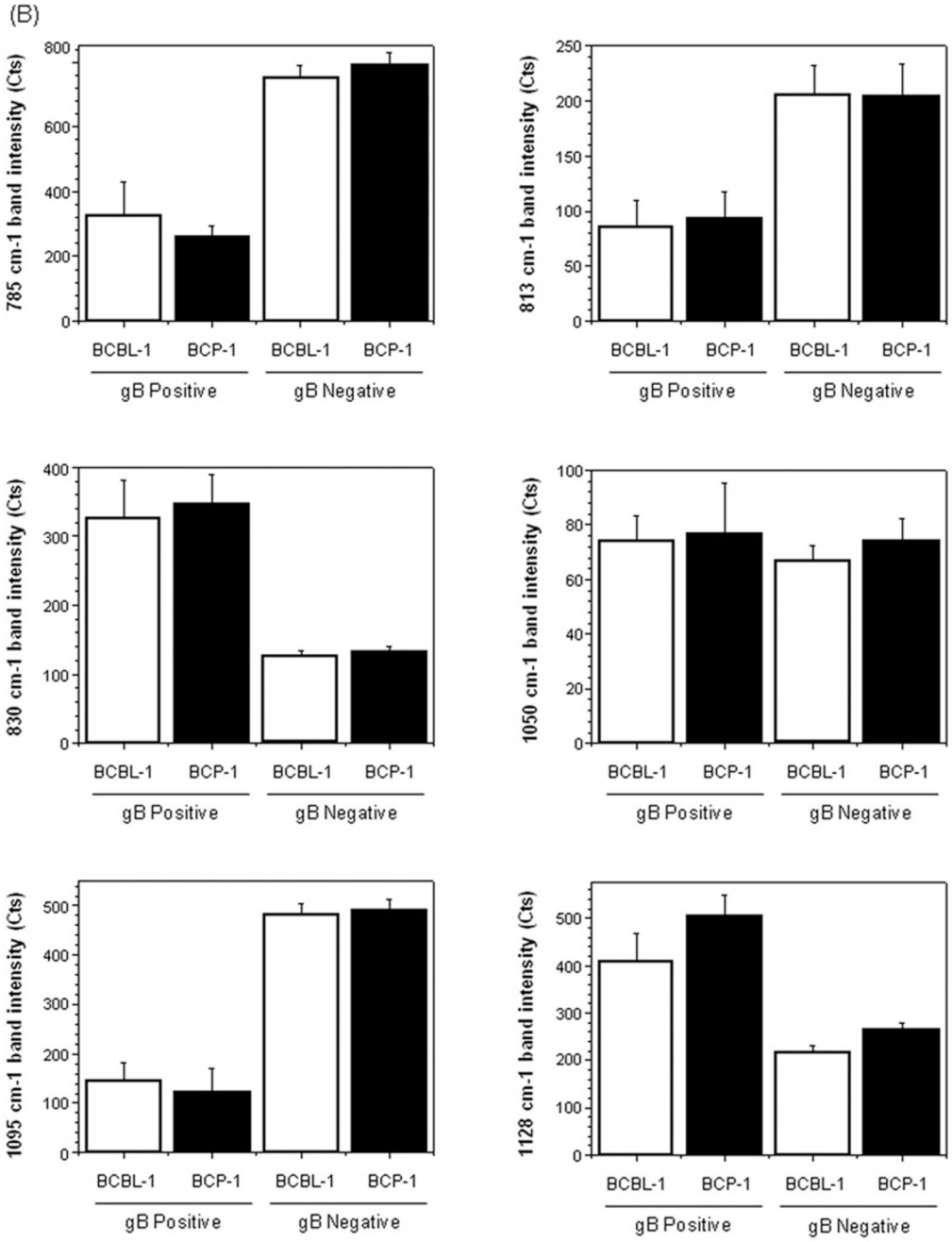

Figure 5. Raman tweezers identifies the unique signature of cells supporting KSHV reactivation

(A) Average Raman spectra of individual BCBL-1 and BCP-1 cells that were actively supporting latent (gB negative) and lytic (reactivation; gB positive) KSHV infection in the fingerprint range from 600 cm^{-1} to 1800 cm^{-1} is provided. Each spectrum was obtained by averaging the spectra of 20 individual cells. **(B)** Spectral changes in 785 cm^{-1}, 813 cm^{-1}, 830 cm^{-1}, 1050 cm^{-1}, 1095 cm^{-1}, and 1128 cm^{-1} Raman bands that occur between target cells supporting a latent and lytic KSHV infection is shown. The spectra are an average of data from 20 cells. Average values on columns with different superscripts are statistically significant ($P<0.05$) by LSD.

Table 1

Raman bands that is unique for KSHV reactivation.

Bands (cm^{-1})	Assigned function	Reference
785*	Phosphodiester bond C'_5-O-P-O-C'_3 (DNA content); and pyrimidine nucleobases (U, T, C)	Chan et al., 2006 [49].
813*	RNA content	Uzunbajakava et al., 2003 [44].
830*	Tyrosine side chains and vibrations in the adenine, thymine 1, and thymine 2 sugars	Meng et al., 2005 [45].
1095*	Phosphodioxy groups PO_2^- of the DNA backbone (DNA content)	Borchman et al., 1999 [47].
1128*	Vibrations of C-N in proteins and C-C in lipids	Notingher et al., 2004 [48].
1050	Indicator of electronic structure of the nucleotides	Chan et al., 2006 [49].

* denotes the five Raman bands that make up the fingerprint of cells supporting KSHV reactivation.